OPEN ACCESS

African Journal of Environmental Science and Technology

July 2023
ISSN 1996-0786
DOI: 10.5897/AJEST
www.academicjournals.org

ACADEMIC JOURNALS
expand your knowledge

About AJEST

African Journal of Environmental Science and Technology (AJEST) provides rapid publication (monthly) of articles in all areas of the subject such as Biocidal activity of selected plant powders, evaluation of biomass gasifier, green energy, Food technology etc. The Journal welcomes the submission of manuscripts that meet the general criteria of significance and scientific excellence. Papers will be published shortly after acceptance. All articles are peer-reviewed

Indexing

The African Journal of Environmental Science and Technology is indexed in:
CAB Abstracts, CABI's Global Health Database, Chemical Abstracts (CAS Source Index), China National Knowledge Infrastructure (CNKI), Dimensions Database, Google Scholar, Matrix of Information for The Analysis of Journals (MIAR), Microsoft Academic

AJEST has an h5-index of 14 on Google Scholar Metrics

Open Access Policy

Open Access is a publication model that enables the dissemination of research articles to the global community without restriction through the internet. All articles published under open access can be accessed by anyone with internet connection.

The African Journal of Environmental Science and Technology is an Open Access journal. Abstracts and full texts of all articles published in this journal are freely accessible to everyone immediately after publication without any form of restriction.

Article License

Memberships and Standards

Academic Journals strongly supports the Open Access initiative. Abstracts and full texts of all articles published by Academic Journals are freely accessible to everyone immediately after publication.

Crossref is an association of scholarly publishers that developed Digital Object Identification (DOI) system for the unique identification published materials. Academic Journals is a member of Crossref and uses the DOI system. All articles published by Academic Journals are issued DOI.

Similarity Check powered by iThenticate is an initiative started by CrossRef to help its members actively engage in efforts to prevent scholarly and professional plagiarism. Academic Journals is a member of Similarity Check.

CrossRef Cited-by Linking (formerly Forward Linking) is a service that allows you to discover how your publications are being cited and to incorporate that information into your online publication platform. Academic Journals is a member of CrossRef Cited-by.

Academic Journals is a member of the International Digital Publishing Forum (IDPF). The IDPF is the global trade and standards organization dedicated to the development and promotion of electronic publishing and content consumption.

Contact

Editorial Office: ajest@academicjournals.org

Help Desk: helpdesk@academicjournals.org

Website: http://www.academicjournals.org/journal/AJEST

Submit manuscript online http://ms.academicjournals.org

Academic Journals
73023 Victoria Island, Lagos, Nigeria
ICEA Building, 17th Floor,
Kenyatta Avenue, Nairobi, Kenya.

Table of Content

Vol. 17(7), pp. 146-156, July 2023
DOI: 10.5897/AJEST2023.3194
Article Number: 77DF6CF70952
ISSN: 1996-0786

http://www.academicjournals.org/AJEST

African Journal of Environmental Science and Technology

Full Length Research Paper

Development of a filter system using silver nanoparticles modified silica sand for drinking water disinfection

Margareth Msoka[1,2], Fortunatus Jacob[2] and Ally Mahadhy[1]*

[1]Department of Molecular Biology and Biotechnology, University of Dar es Salaam, Tanzania, P. O. Box 35179 Dar es salaam, Tanzania.
[2]Chemistry Department, University of Dar es Salaam, Tanzania, P. O. Box 35061 Dar es salaam, Tanzania.

Received 12 May, 2023; Accepted 27 June, 2023

This study presents a filter system for the removal of pathogenic microorganisms from potable water using silver nanoparticle-modified silica sand. While silica sand has potential applications in wastewater treatment, its effectiveness in microbial filtration falls short. Thus, there is a need for an environmentally friendly enhancement method. The silver nanoparticles were synthesized using *Commelina maculata* leaf extracts, and their diameter ranged from 50 to 80 nm. The Ag NPs were immobilized on silica sand, improving the modified sand's physicochemical properties. The filter system, composed of Ag NP-modified silica sand packed in a glass column, reliably removed 98% of the culturable *E. coli* population in water. The results suggest that the developed filter system has potential use in drinking water disinfection in remote rural areas. However, further cost analysis is required before scaling up for mass production and real-world use.

Key words; Silver nanoparticles, silica sand, *Commelina maculate*, microbial filtration, water treatment.

INTRODUCTION

Availability of safe drinking water is a major concern in Sub-Sahara African countries, with significant implications for public health and economic development. Water-borne diseases such as cholera, typhoid, and diarrhoea are prevalent, particularly in rural areas where families often rely on rivers and unprotected sources for domestic water needs. Despite efforts to promote household water treatment, only 18.2% of families treat their drinking water at home, contributing to the recurrence of water-borne infections (Sugumari et al., 2021). Additionally, poor construction and maintenance of water systems, damaged infrastructure, and a lack of hygiene and sanitation knowledge in urban areas also lead to water contamination and associated health risks (Sadhana, 2016).

Silica sand is a common water filtration medium that has been used for over 150 years due to its inert and non-toxic nature. This inertness ensures that the sand does not introduce unwanted chemical into the water supply (Lavon and Bentury, 2015). However, the effectiveness of silica sand in removing contaminants from potable water is limited. Recent efforts to improve the effectiveness of silica sand filtration have focused on modifying the sand with chemically synthesized

*Corresponding author. E-mail: allymahadhy@yahoo.com. Tel: +255 656 133 034.

nanoparticles, which have shown promise in purifying drinking water (Munasir et al., 2020). However, conventional nanoparticle synthesis methods involve the use of toxic and hazardous chemicals, presenting significant environmental and health risks (Das et al., 2017).

Green synthesis of metallic nanoparticles using natural sources such as plants, animals, and microorganisms has emerged as a promising alternative approach (Das et al., 2017). Compared to chemical synthesis, these green synthesis methods can produce nanoparticles with lower toxicity and have fewer environmental impacts. In this study, a novel water treatment technology was developed, utilizing silica sand filters modified with non-toxic, green-synthesized nanoparticles derived from *Commelina maculata.* This plant, belonging to the *Commelinaceae* species, is readily available and is a small, perennial herbal plant mostly found in wet places. *Commelina maculata* offers a favourable environment for nanoparticle synthesis as it is free from toxic chemicals and provides natural capping agents (Shah et al., 2017). The extract of *Commelina maculata* has been shown to produce silver nanoparticles without toxicity, unlike their chemically synthesized counterparts (Eranga et al., 2017). This approach has the potential to offer an effective, efficient, and affordable means of achieving nanoparticles for water treatment and purification. Overall, the use of green-synthesized nanoparticles for water treatment is a promising approach that can potentially be employed in various fields, including environmental, biomedical, agricultural, and electronics.

MATERIALS AND METHODS

Materials

Fresh leaves of *Commelina maculate* and silica sand were obtained from two different locations in Tanzania: the vegetation at Mwalimu JK Nyerere campus of the University of Dar es Salaam (UDSM) at 6.77580S, 39.20900E and the seashore at Kigamboni in Dar es Salaam (6.82270S, 39.30240E) respectively. A glass column with a diameter of 1.5 cm and a length of 25 cm was fabricated at the UDSM Central Science Workshop. All chemicals utilized in the study were of analytical grade, procured from Sigma-Aldrich, and employed as received without undergoing any additional purification.

Methods

Preparation of plant extract

To prepare the plant extract, the method described in (Archana et al., 2021) was followed with minor modifications. Firstly, fresh leaves were thoroughly washed with distilled water to eliminate any dust particles and then air-dried at room temperature for one day. Next, 10 grams of the dried leaves were measured and ground into a smooth powder.

The powdered sample was then heated with 200 mL of sterile distilled water at 60°C for 5 min, and allowed to cool to room temperature. The sample was then filtered through a Chm No. F1001 filter paper, and the filtrate was collected. To remove any heavy biomaterials present, the collected filtrate was centrifuged at 3000rpm for 15 min.

Biosynthesis of silver nanoparticles

To synthesize silver nanoparticles, a 1 mM solution of silver nitrate (AgNO3) in 100 mL volume was prepared. 50 mL of an aqueous leaf extract of *Commelina maculate* species, which had been prepared beforehand using the method described in the (Archana et al., 2021) publication with minor adjustments, was added to the silver nitrate solution. The resulting mixture was then incubated in a dark and undisturbed environment at room temperature for 3 h, which led to the formation of silver nanoparticles.

Modification of silica sand with silver nanoparticles

To prepare the Ag NPs-modified silica sand, 100 grams of clay-free silica sand with average grain diameters of 420 µm, 3360 µm, and 4760 µm were measured individually and washed with water. Each sand sample was then soaked in 50 mL of Ag NPs suspension for 24 h, washed several times with distilled water, and oven-dried for 3 h. The dried sand samples were stored in a desiccator.

To set up the column, a glass column with a length of 25 cm and a diameter of 1.5 cm was clamped vertically. The column was then filled with the Ag NPs-modified silica sand. To prevent sand from leaking out of the lower end of the column, a 1 cm thick sterilized cotton wool was used to plug the column.

Determination of bacterial removal efficiency of the packed column

Two distinct operational modes were employed to examine the effectiveness of a column packed with Ag NPs-modified silica sand for microbiological water treatment. The first mode was a continuous flow system that utilized a peristaltic pump, and the second mode was a batch setup system driven by gravitational force. In each case, four separate beakers were filled with 100 mL of sterile water samples, and 1, 2, 4- and 10-mL volumes of nutrient broth containing 1.5×10^8 Cfu/mL bacteria (either *E. col*i or *S. typhi*) were transferred into each beaker. Subsequently, 2 mL of well-mixed contaminated water was extracted from each beaker to establish the initial bacterial concentration. The remaining contaminated water (about 98 mL) was then passed through the column either in continuous flow mode with a flow rate of 55.6 µL/s or in batch mode. After passing through the column, 2 mL of treated water was sampled from each beaker to determine the concentration of bacteria in the treated water.

To assess the effectiveness of the packed column, real water samples were collected from two different sources: stream water from the Academic Bridge at the Mwalimu J.K Nyerere campus of UDSM and tap water from the Chemistry laboratory at UDSM. The water samples were collected in 2 L sterilized polypropylene containers and their initial bacterial concentrations were determined. The bacterial concentration in the water samples was measured before and after treatment using two methods. The first method involved measuring the absorbance of the samples at a wavelength of 60 nm using spectrophotometry. The absorbance was directly proportional to the bacterial concentration in the sample. The second method involved determining the bacterial concentration in agar plates at 37°C for 24 h using the colony forming unit method. All experiments were conducted in triplicate.

The viability of bacteria (*E. coli* and *S. typhi*.) in the water samples before and after treatment was also determined using an indicator dye called p-iodonitrotetrazolium (INT) at a concentration of 0.2 mg/mL (40 µL). The dye changes from colourless to pink

Figure 1. Aqueous Leaf Extract, Aqueous Synthesized *C*-Ag NPs and its Solid Synthesized *C*-Ag NPs.
Source: Authors

when in contact with living microorganisms.

RESULTS AND DISCUSSION

Biosynthesis of silver nanoparticles

A yellowish-brown colour solution was developed following mixing of silver ions with leaves extract (Figure 1). The successful synthesis of silver nanoparticles in a reaction mixture can be detected by the presence of a yellowish-brown colour. This colour is caused by the surface plasmon vibrations in the nanoparticles, as explained in a study by Protima et al. (2014). The reduction of silver ions by leaf extracts to form Ag NPs was confirmed by scanning the absorption maxima at the wavelength range from 200–700 nm using, SPECORD 210 PLUS UV-Vis spectrophotometer by Konrad Zuse Strasse1, Germany found at University of Dar es salaam Chemistry Department. The results showed a sharp surface plasmon band centred at 445 nm, which is a characteristic peak for silver nanoparticles. This peak falls within the range of 420-450 nm, which is typical for silver nanoparticles, as reported by Kero et al. (2017). In contrast, a control sample of leaf extract did not exhibit a peak at 445 nm, but rather showed a peak at 309 nm (Figure 2b), indicating the absence of silver nanoparticles in this solution, as noted by Kero et al. (2017).

Characteristics of plant extract and synthesized silver nanoparticles

Chemical composition of commelina maculate (plant) extract and the reaction mixture

To identify the chemical composition of the *Commelina maculate* extract and the compound responsible for reducing, capping, and stabilizing the synthesized silver nanoparticles, FT-IR spectroscopy was used. The IR spectra were recorded by Perkin-Elmer 2000 FTIR spectrometer from America which found in UDSM Chemistry Department in the wavenumber range of 4000 cm^{-1} to 500 cm^{-1}. The FT-IR spectral results for (a) the Commelina extract and (b) the reaction mixture after the completion of the biosynthesis of Ag NPs are presented in Figure 3. Additionally, the technique was used to confirm the presence of silver nanoparticles.

The FTIR spectra presented in Figure 3 indicate that the Commelina extract contains molecules of different functional groups, such as hydroxyl and carbonyl groups. Specifically, Figure 3 (a) shows bands for the Commelina

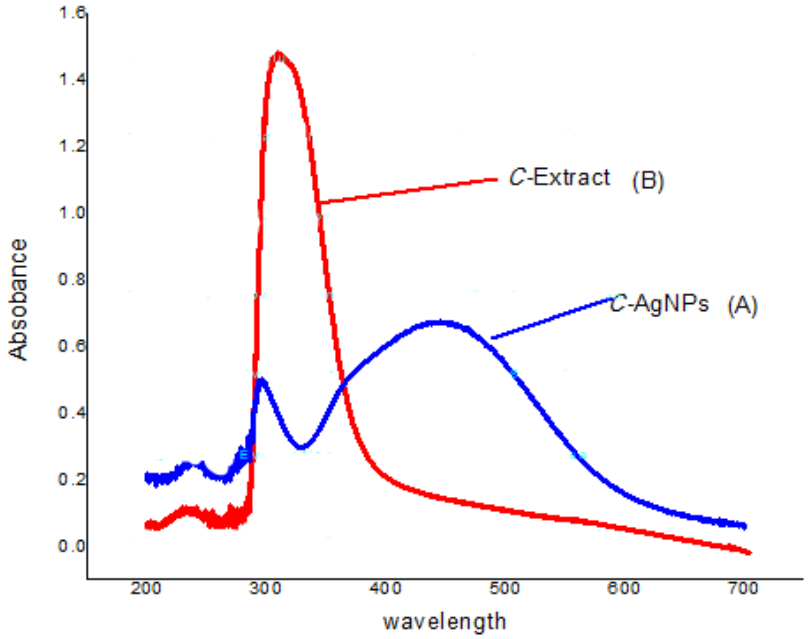

Figure 2. Showing UV-Vis Spectral Scans of the Reaction Mixture, *Commelina*-Ag NPs (A) and Control Sample, Plant Extract (B).
Source: Authors

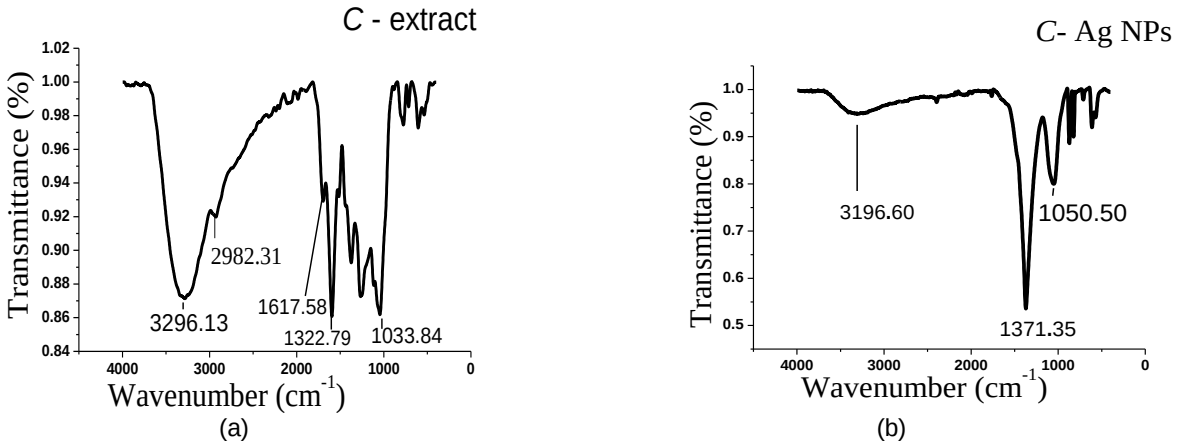

Figure 3. FTIR spectral scan of (a) Commelina extract and (b) biosynthesised Ag NPs**.**
Source: Authors

extract at 3296.13 cm-1, 1617.58 cm-1, 1322.79 cm-1, and1033.84 cm-1, while Figure 3 (b) shows bands for the reaction mixture (C-Ag NPs) at 3201.60 cm-1, 1371.35 cm-1, and 1050.50 cm^{-1}.

The band at 3296.13 – 3201.60 cm^{-1} corresponds to a strong O-H stretching vibration, which indicates the very likely presence of phenols and alcohols (Petkovic, 2011). Furthermore, the peak at 1033.84 cm-1 in the Commelina extract and the peak at 1050.50 cm-1 in the C-Ag NPs sample are attributed to the O-H of, most likely, the phenols, which are believed to aid in the reduction of Ag^{+} into Ag^{0} through the sharing of polyphenols, such as flavonoids and terpenoids.

The phenolic compounds such as lignin, phenolic acids, tannins, and stilbenes are responsible for the rapid reduction along with stabilizing and capping of silver ions into silver nanoparticles (Adhikari et al., 2022) On the other hand, the band at 1617.58 – 1322.79 cm^{-1} corresponds to amide group, which is a protein peptide bond (Yan et al., 2014). The absorption bands displayed

by the amides are usually due to N-H and C=O, C-C and to some extent from the C-N stretching vibrations. Accordingly, the peak observed at 1617.58 cm^{-1} in *Commelina* extract was designated for C-C and C-N stretching vibrations, indicating the presence of protein molecules. The peaks at 1322.79 cm^{-1} in *Commelina* extract and 1371.35 cm^{-1} in C-Ag NPs, were assigned for the proteins N-H vibration and N-H stretching vibrations, respectively.

These bonds usually present in the amide linkage of the proteins. In addition to the backbone amide modes, the bands at 1033.84 cm^{-1} and 1050.50 cm^{-1} regions, which are observed in *Commelina* extract and C-Ag NPs, respectively, contain absorption from many functional groups relevant to proteins and their side-chains (Huyan et al., 2015).

Therefore, these results suggest the presence of phenolic and protein molecules in both *Commelina* extract and C-Ag NPs samples. However, the letter was suggested to contain fewer phenolic and proteins molecules. This can be attributed to their involvement in the reduction and stabilization of synthesized Ag NPs, which is evidently by the slight variations in the O-H and N-H peaks patterns between the two samples and the disappearance of the band at 1617.58 cm^{-1} for C-C and C-N in C-Ag NPs sample.

Topographical and morphological characteristics of biosynthesised silver nanoparticles

AFM analysis

The topographical and morphological features of nanoparticles play a crucial role in determining their properties. These features include various factors such as size, shape, distribution, localization, agglomeration/ aggregation, surface morphology, surface area, and porosity of the nanoparticles, which collectively influence their behaviour (Stefanos et al., 2018). To examine the topographical and morphological characteristics of Ag NPs in this study, AFM was used. The synthesized silver nanoparticles were characterised by AFM digital instrument MMAFM-2 (Illinois, U.S.A) in the department of Physics at the University of Dar es salaam. Figure 4 illustrates the size and disparity of the particles.

The AFM analysis revealed that the biosynthesized silver nanoparticles (C-Ag NPs), produced using *Commelina maculate* extract, were spherical in shape and had a variable size range of 2 to 90 nm, with an average grain size of 51.36 nm. Despite being polydisperse, some agglomeration of C-Ag NPs was observed, which could be attributed to the magnetic properties of the individual silver particles or subunits. In some instances, particles larger than 100 nm were also observed, which might be due to the agglomeration caused by reaction parameters, such as the amount of reducing agent, as suggested by Yasser et al. (2017). Similar findings have been reported in a study by Periasamy et al. (2022), where silver nanoparticles synthesized using Hibiscus rosasinensis leaf extract showed analogous results.

XRD analysis

The structural analysis of the synthesized Ag NPS was conducted by using X-ray diffractometer BTX SN 231(Kyoto, Japan) equipped with Co-kα radiation source to examine the crystalline nature of the biosynthesized C-Ag NPs. The X-ray diffraction (XRD) pattern was measured by drop coated films of Ag NPs of each sample on metal plate and employed with characteristic radiation in the range of 10–50^{o} at a scan rate of 0.05/min with the time constant of 2 s, Co-Kα radiation and amplitude wave k = 1.79 Å working with a 30.5 kV voltage and 0.340 mA current. The full-width at half-maximum (FWHM) from five different peaks were used in Debye- Scherrer's equation to determine the average crystallite size of the nanoparticles (Raman et al., 2012).

The resulting XRD pattern (Figure 5) displayed six distinct reflections at specific angles: 22.74°, 26.32°, 37.58°, 44.40°, 46.46°, and 54.21°. These angles corresponded to Miller indices [hkl] (111), (109), (101), (204), (202), and (006) respectively, indicating a face-centred cubic configuration and a nanocrystalline structure for the particles. This finding aligns with the work of Khan et al. (2011). Importantly, no additional reflections beyond the Ag lattice were observed, suggesting that the biosynthesized C-Ag NPs are highly stable and unaffected by other molecules present in the *Commelina maculate* leaf extract.

Antibacterial activity

The disc diffusion method was employed to assess the antibacterial efficacy of the synthesized Ag NPs against two common waterborne pathogens: *E. coli* (ATCC 25922) and *Salmonella typhi* (*S. typhi*) (ATCC 19430). Erythromycin, a standard antibiotic, served as the positive control for the test pathogens. The results indicated that Ag NPs at a concentration of 40 mg/mL exhibited excellent antibacterial activity against both *E. coli* (21.7±0.2 mm) and *S. typhi* (19.3±0.1 mm), as evidenced by the zone of inhibition (ZOI) surrounding the discs. Figure 6 displays the ZOI of C-Ag NPs against each tested pathogen: (a) *E. coli* and (b) *S. typhi*. Table 1 shows antibacterial activity for synthesized Ag NPs and plant extract**.**

After conducting several dilutions of the synthesized Ag NPs, the minimum inhibitory concentration (MIC) was found to be 0.054062 mg/ml for *E. coli* and 0.05750 mg/ml for *S. typhi*. This finding aligns with the observation made by Espinosa et al. (2009) that smaller nanoparticles

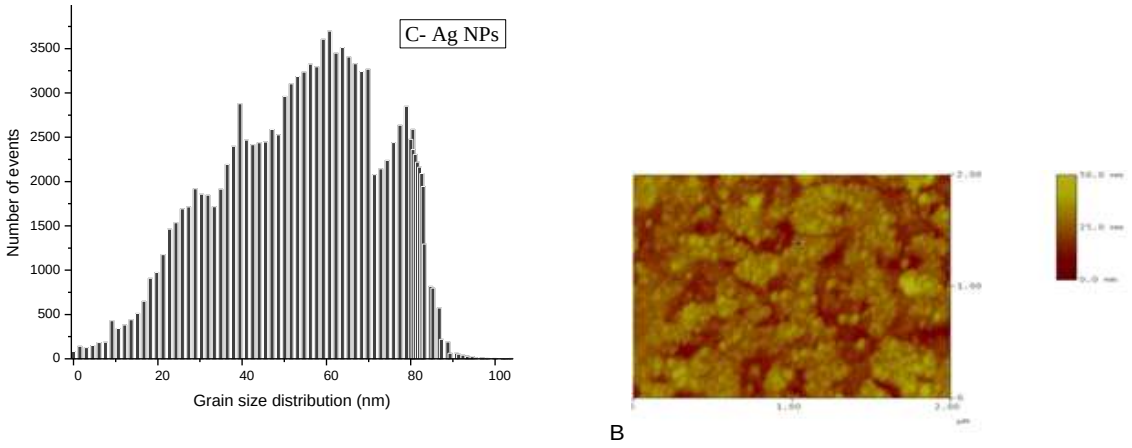

Figure 4. Particle Size Distribution of Ag NPs Synthesized by *Commelina* extract.
Source: Authors

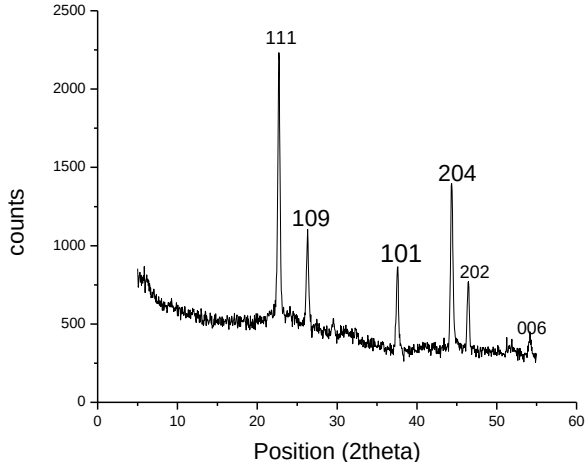

Figure 5. Depicting the X-ray diffraction pattern of crystalline nature of C-Ag NPs.
Source: Authors

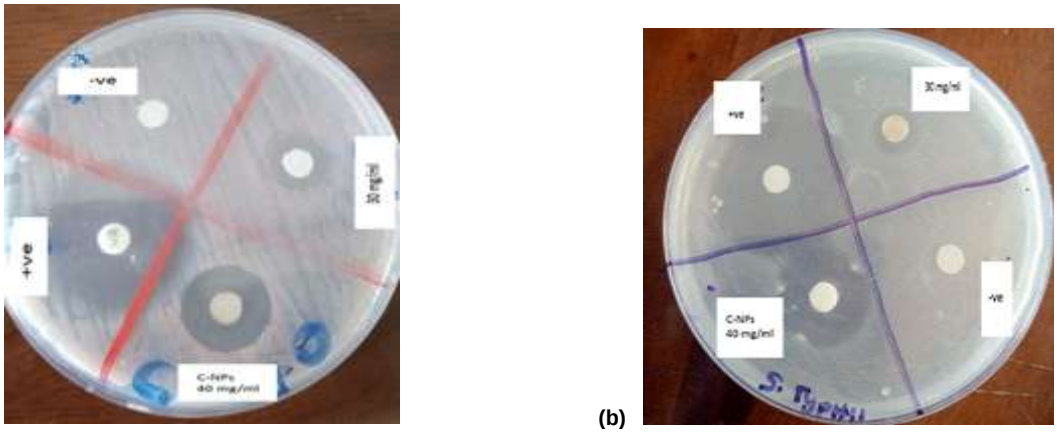

Figure 6. Antibacterial assay showing inhibition zone of 40 mg/ml C-Ag NPS against (a) *E. coli* and (b) *S. typhi.*
Source: Authors

Table 1. Antibacterial Activity for Synthesized Ag NPs and plant extract**.**

Sample		Zone of inhibition (mm)	
Type	**Concentration (mg/mL)**	***E. coli***	***S. typhi***
C-Ag NPs	30	13±0.1	12±0.1
C-Ag NPs	40	21.7±0.2	19.3±0.1
C-extract (100%)	ND	0.0±0.0	0.0±0.0
Erythromycin (+ve control)	5×10^{-4}	31.3±0.5	32.7±0.2
Sterile water (-ve control)	ND	0.0±0.0	0.0±0.0

Source: Authors

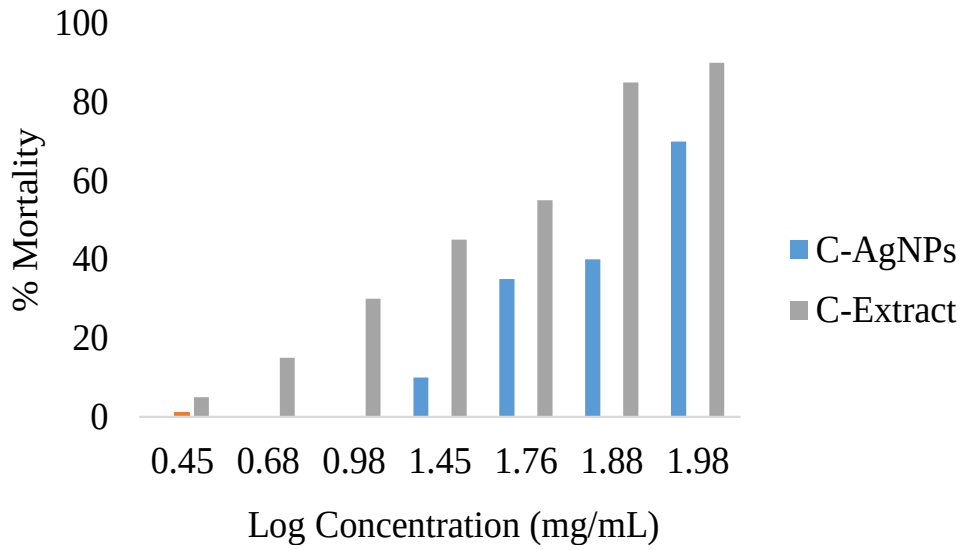

Figure 7. Showing Mortality Rate of Brine shrimp larvae Due Toxicity Effect of Plant Extract and Synthesized Ag NPs against Brine Shrimp larvae.
Source: Authors

have a lower MIC compared to larger ones. The synthesized Ag NPs exhibited an 80% minimum inhibition concentration at an optimal bacterial concentration of 10^6 Cfu/mL, as reported by Retan et al. (2011). These results demonstrate the potential of *Commelina maculate* leaf extract as a valuable ingredient in nanotechnology for inhibiting various microorganisms and its application in water treatment.

Toxicity analysis

The *Commelina* extract and synthesized silver nanoparticles (C-Ag NPs) were studied for their toxicity using brine shrimp lethality bioassay (Figure 7).

The study found that both the Commelina extract and C-Ag NPs did not exhibit toxicity even at high concentrations. The LC50 values, which represent the concentration at which 50% of cells are killed, were 107.0 mg/ml and 44.0 mg/ml after 24 h for the extract and NPs, respectively. A sample with an LC50 value above 0.1 mg/ml is considered non-toxic. These findings are consistent with previous studies such as Zan et al. (2020) and Zhou et al. (2018). Therefore, the study concludes that the Commelina extract contains biochemical compounds that can be used for the green synthesis of non-toxic Ag NPs, which have potential applications in disinfecting drinking water.

Application of synthesized Ag NPs in disinfection of water

Immobilization and characterization of Ag NPs on silica sand

The synthesized silver nanoparticles were immobilized on 3360 µm silica sand (Figure 8). Upon immobilization with Ag NPs, the colour of the silica sand changed from white to brown. Approximately 0.905 µg of Ag NPs was found

Figure 8. Presenting Natural Silica Sand Before and After Immobilization with Ag NPs.
Source: Authors

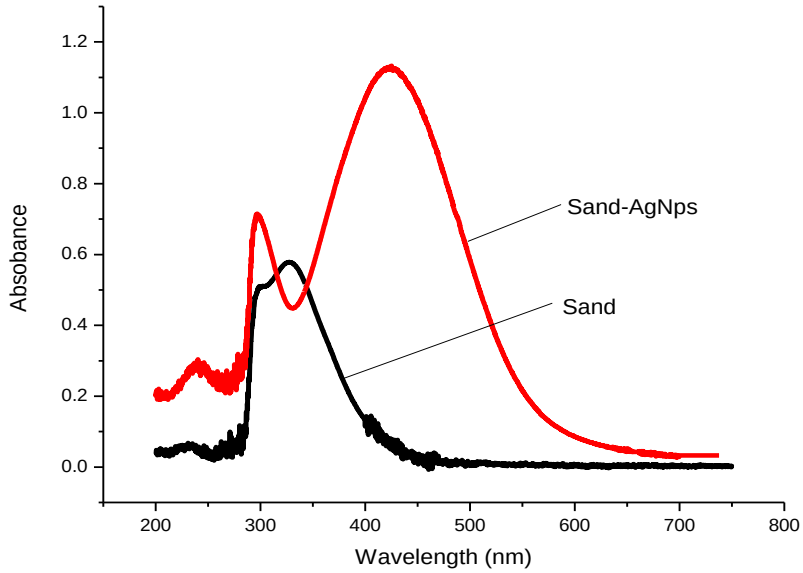

Figure 9. The UV-Vis absorption spectrum for Ag NPs-immobilized and non-immobilized silica sand.
Source: Authors

in every 100 g of immobilized silica sand. The presence of Ag NPs on the surface of the immobilized silica sand was analysed using UV-vis spectrophotometry. The results indicate that the silica sand contains silver nanoparticles, as evidenced by the UV-vis absorption peak remaining within the peak region at a wavelength of 438 nm, even after several washings with sterile water (Figure 9).

The structural features of Ag NPs-immobilized silica sand surface were characterized by AFM using an 80 µm scan range. The immobilized sand was scanned 2 mm to the left and 10 mm to the right, as described by Rao et al. (2007). Surface texture parameters were calculated to evaluate the differences in the topographical surface of the silica sand before and after immobilization with Ag NPs. The roughness parameters (average roughness Ra, root mean square roughness Rq, maximum roughness Ry, and maximum profile peak height Rp, and roughness skewness Rsk) of the silica sand surface before and after immobilization with Ag NPs are presented in Table 2.

The results indicate a decrease in the roughness parameters of silica sand after immobilization with Ag

Table 2. Roughness parameters of silica sand before and after immobilization of Ag NPs.

Sample	R_a(nm)	R_q (nm)	R_y (nm)	R_p (nm)	R_{sk}
Sand before	134.2	161.2	400.8	248.1	423.4
Sand after	59.2	86.3	267.7	108.2	198.2

Source: Authors

NPs, suggesting the presence of a smoother surface. This smoother surface is likely a result of the even distribution of the immobilized Ag NPs on the silica sand. Similar observations have been reported in previous studies involving the immobilization of Ag NPs on silica sand or other surfaces (Alena et al., 2014).

Assessment of Ag NPs-Silica sand filter performance for bacteria removal in water

The performance of the silica sand-Ag NPs filter for bacteria removal in water was determined spectrophotometrically by measuring the optical density (OD) of water before and after passing through the column at 600 nm. Three different water samples were examined: (i) water contaminated with a known volume of bacterial culture, (ii) tap water, and (iii) stream water. It has been established that absorbance is directly proportional to the concentration of matter in the sample and is determined by the amount of light scattered in the water sample (Buchanan et al., 2017). Therefore, the higher the number of bacteria in the water sample, the higher the recorded absorbance on the spectrophotometer. Additionally, the presence of microorganisms in the water was also determined using an indicator called p-iodonitrotetrazolium (INT).

The study was conducted in two different experimental setups: batch and continuous flow modes. In the continuous flow mode, a silica sand filter without Ag NPs (non-modified silica sand filter) was used as a control setup.

The optical densities of all water samples were observed to decrease after treatment with Ag NPs-silica sand filters in both, batch and continuous flow modes, suggesting the effective removal of bacteria in the water samples. The same water samples, before and after treatment, was subjected to bacterial culturing; faecal coliforms were detected in all samples before treatment, but were not detected in treated ones. These results indicate that the entire treatment process is capable of removing bacteria, especially faecal coliforms which are the mostly causative of waterborne infection (Suvadhan, 2014). It has long been known that sand has been used as a filter to purify drinking water in many industry (Saad et al., 2016), and silica sand has been used to purify water as it has ability to trap microorganism (Rafael, 1992).

However, the contribution of Ag NPs in bacterial removal from water sample is clearly demonstrated in this study by the observed smaller change in optical density of water samples treated with unmodified (control) silica sand filter compared to Ag NPs-modified silica sand filter. For instance, the optical density decreases of 6 and 97% were recorded for stream water treated with control and Ag NPs-modified silica sand filters, respectively. In other words, the column packed with Ag NPs-modified silica sand has more than 10 times bacterial removal capacity than the one packed with unmodified silica sand (control).

The contribution bacterial removal effect of Ag NPs can be attributed to the adsorption affinity of the reduced silver towards the bacterial cell wall (Shkodenko et al., 2020). Either, the presence of viable bacteria in the same water samples was determined by using an indicator dye, *p*-iodonitrotetrezolium (INT). All water samples changed the colour, from colourless to pink, upon addition of INT dye. However, no colour change was observed in any water sample after treatments.

Silver nanoparticles are well known to have the ability of penetrating bacterial cell walls, destroying the cell membranes and even resulting in cell death. Their efficacy is contributed by both, their nanoscale size nature and large surface area to volume ration properties (Linlin et al., 2017). Moreover, continuous flow showed to be more effective (97%) in bacterial removal from tap/stream water samples than the batch mode (93%), This is because the water in continuously filter being fluffed and swirl in an upflow design since it has more contact with the filter media thus produce better results (Brastad et al., 2013). While the use of batch mode depends on gravitational force, water flow may push through the device without significant interaction with the media (Linlin et al., 2017). Furthermore, drinking water is not expected to contain detectable amounts of Ag+/Ag NPs; if found, it is considered to be contamination (Gupta et al., 2019).

Leakage/leaching of Ag NPs in treated water were also determined. The amount of Ag NPs in treated water was found to be 3.87 femtogram (fg)/L of the collected water sample after treatment. However, no further leaching was observed after passing the first 100 ml, and the column retains almost all Ag NPs on the surface (> 99.95). This explains that, Ag NPs coated/immobilized on silica sand are stable and firmly adsorbed on the sand surface, allowing them to work with high efficiency and at minimum cost compared to other commonly used methods such as

ozonation, which require vast amounts of energy and capital (Naicker et al., 2023). The World Health Organisation (WHO) recommends that the maximum allowable concentration of silver in drinking is 0.1 mg/L (WHO, 2017), which is extremely higher, about 10^{11}, than the one recorded in this study. Typically, silver concentrations in surface water and groundwater are observed to be below 2 µg/L (ATSDR, 1990). On average, the concentrations of silver in these natural water sources have been documented to range from 0.2 to 0.3 µg/L (UEPA, 1980). Furthermore, neither faecal coliforms nor *E. coli* was detected in the filtered water by developed column. The absence of both faecal coliforms and E. coli in the filtered water, despite their detection in the original water sample, demonstrates the efficacy of the entire treatment process in removing bacteria. This is particularly significant for faecal coliforms, which are commonly associated with waterborne infections and pose a significant health risk (Forstinus et al., 2016).

Conclusion

Overall, this study highlights the potential of using green synthesis methods to produce bio-functional and non-toxic Ag NPs, which can be used for disinfection of drinking water. The use of locally available plants, such as *Commelina maculate*, makes the process more sustainable and cost-effective. The Ag NPs-modified silica sand filter demonstrated a high bacterial removal efficiency of 98% while maintaining minimal Ag NPs leakage. However, further studies are required to assess the long-term stability and effectiveness of the filter under different water treatment conditions. Overall, this approach holds promise as a safe and effective method for providing access to clean drinking water in regions with limited resources

CONFLICT OF INTERESTS

The authors have not declared any conflict of interests.

REFERENCES

Archana KM, Rajagopal R, Krishnaswamy VG, Aishwarya S (2021). Application of Green Synthesied Copper Iodide Particle on Cotton Fabric-Protective Face Mask Material against COVID-19 Pandemic. Journal of Materials Research and Technology 15:2102-2116.

Adhikari A, Chhetri K, Acharya D, Pant B, Adhikari AD (2022). Green synthesis of Iron Oxide nanoparticles using Psidium Gwajava Leaves Extract for Degradation of Organic dye and Antmicrobial Application. Catalysts 12(10):1188-1191.

Agency for Toxic Substances and Disease Registry (ATSDR) (1990). Toxicalogical Profile for Silver.

Alena R, Zdnka N, Zdenk K (2004). Immobilization of Silver Nanoparticles on Polythylene Terephthalate. Journal of Nanoscale Research 10:305-315.

Brastad KS, He Z (2013). Water Softening Using Microbial Desalination Cell Technology. Desalination 309:32-37.

Buchanan CM, Wood RL, Hoj TR, Alizadeh M, Bledsoe CG, Wood ME, McClellan DS, Blanco R, Hickey CL, Ravsten TV, Husseini GA (2017). Rapid Separation of Very Low Concentration of Bacteria from Blood. Journal of Microbiological Methods 139:48-53.

Das RK, Pachapur VL, Lonappan L, Naghdi M, Pulicharla R, Maiti S, Cledon M, Dalila LM, Sarma SJ, Brar SK (2017). Biological synthesis of metallic nanoparticles: plants, animals and microbial aspects. Nanotechnology for Environmental Engineering 2:1-21.

Eranga R, Chanica J and Dulashin R (2017). Honey Mediated Green Synthesis of Nanoparticles. Journal of Nanomaterials 3:118-139.

Forstinus N, Ikechukwu N, Emenike M, Christiana A (2016). Water and waterborne diseases: A review. International Journal of Tropical Disease and Health 12(4):1-4.

Gupta S, Khare D, Mishra N, Sharma AK (2019). Waste water parameters and its Imperishable Augmentation.

Kero J, Sandeep B, Sudhakar P (2017). Synthesis, Characterization, and Evaluation of the Antibacterial Activity of Allophylus serratus Leaf and Leaf Derived Callus Extracts Mediated Silver Nanoparticles. Journal of Nanomaterials.

Khan Z, Hussain JI, Kumar S, Hashmi AA, Malik MA (2011). Silver Nanoparticles Green Route Stability and Effect of Additives. Journal of Biomaterials and Nanobiotechnology 2(4):390.

Lavon O, Bentury Y (2015). Silica Gel: Non-Toxic Ingestion with Epidemiologic and Economic Implications. The Israel Medical Association Journal 17(10):604-606.

Linlin W, Chen H, Longquan S (2017). The antimicrobial activity of nanoparticles: present situation and prospects for the future. International Journal of Nanomedicine 7:1227-1249.

Munasir M, Hidayat N, Kusumawati DH, Putri NP, Taufiq A, Sunaryono S (2020). Amorphous-SiO2 nanoparticles for water treatment materials. In AIP Conference Proceedings 2251(1) AIP Publishing.

Naicker KI, Kaweesa P, Daramola MO, Iwarere SA (2023). Non-Thermal Plasma Review: Assessment and Improvement of Feasibility as a Retrofitted Technology in Tertiary Wastewater Purification. Journal of Applied Sciences 13(10):6243.

Periasamy S, Jegadeesan U, Sundaramoorthi K, Rajeswari T, Tokala VN, Bhattacharya S, Muthusamy S, Sankoh M, Nellore MK (2022). Comparative analysis of synthesis and characterization of silver nanoparticles extracted using leaf, flower, and bark of hibiscus rosasinensis and examine its antimicrobicidal activity. Journal of Nanomaterials 10:812-854.

Petkovic M (2011). O–H stretch in phenol and its hydrogen-bonded complexes: band position and relaxation pathways. The Journal of Physical Chemistry 116(1):364-371.

Protima R, Erwa R, Stanislav F and Mangala P (2014). Silver nanoparticles: Synthesis and Application. Journal of Advanced Research 4:2-9.

Rafael G (1992). Ripening of Silica Sand Used for Filtration. Water Research 1:10-19.

Raman N, Sudharsan S, Veerakumar V, Pravin N, Vithiya K (2012). Pithecellobium dulce mediated extra-cellular green synthesis of larvicidal silver nanoparticles. Spectrochimica Acta Part A: Molecular and Biomolecular Spectroscopy 96:1031-1037.

Rao A, Schoenenberger M, Gnecco E, Glatzel T, Meyer E, Brändlin D, Scandella L (2007). Characterization of nanoparticles using atomic force microscopy. InJournal of Physics: Conference Series 61(1):971.

Retan D, Gang S, Nath SS (2011). Preparation and Antibacterial Activity of Silver Nanoparticles. Journal of Biomaterials and Nanobiotechnology 2(4):472.

Saad FNM, Jamil1 MN, Odli ZSM, Izhar TNT (2016). Study on Modification Towards Water Quality of Wet Market Waste Water. MATEC Web of Conferences 78:101104.

Sadhana C (2016). Traditional Water Purification Methods used in Rural area. Department Energy Environmental 8:12-33.

Shah MD, D'souza UJ, Iqbal M (2017). The potential protective effect of *Commelina nudiflora* L. against carbon tetrachloride (CCl4)-induced hepatotoxicity in rats, mediated by suppression of oxidative stress and inflammation. Environmental Health and Preventive Medicine 22(1):1-9.

Shkodenko L, Kassirov I, Koshel E (2020). Metal Oxide Nanoparticles Against Bacteria Biofilm: Perspectives and Limitations. Microorganisms 8(10):1545.

Stefanos M, Rogers M, Nguyen T (2018). Characterization Techniques for Nanoparticles: Comparison and Complementary upon Studying Nanoparticles Properties. Journal of Nanoscale 4:12871-12934.
Sugumari V, Krisha S, Khangton S (2021). Development in Magnetic Nanoparticles and Nano-compostite for Wastewater Treatment. Journal of Jece 7:116-132.
Suvadhan K (2014). Nanotechnology for Water Treatment. International Journal of Environmental Analytical Chemistry4:41-72.
United States Environmental Protection Agency (UEPA) (1980). Ambient Water Quality Criteria for Silver. Report Number. EPA 440/5-80-071. Environmental Protection Agency, USA.
World Health Organization (WHO) (2017). Drinking Water quality 4th Edition. Incorporating the 1st Addendum 1:1-10.
Yan J, Yang X, Ying Q (2014). Poly-Amidoamine Structures Characterization: Amide Resource Structure Imidic Acid and Tertiary Ammoniaum. Journal of Advanced Research 1:16-90.
Yasser Z, Kyong Y, David H (2017). Influence of Nanoparticles aggregation/ Agglomeration on the Interfacial and Tensile Properties of Nanocomposite. Journal of Computer Part B. Engineering 4:10-12.
Zan K, Chen XQ, Zhao MB, Jiang Y, Tu PF (2020). Cytotoxic sesquiterpene lactones from Artemisia myriantha. Phytochemistry Letters 37:33-36.
Zhou X, Friedmann KS, Lyrmann H, Zhou Y, Schoppmeyer R, Knörck A, Mang S, Hoxha C, Angenendt A, Backes CS, Mangerich C (2018). A Calcium Optimum for CytotoxicT Lymphocyte and natural Killer Cell Cytotoxicity. The Journal of physiology 596(14):2681-2698.

Vol. 17(7), pp. 157-166, July 2023
DOI: 10.5897/AJEST2022.3173
Article Number: 89512A871035
ISSN: 1996-0786

http://www.academicjournals.org/AJEST

African Journal of Environmental Science and Technology

Full Length Research Paper

Impact of climate variability modes on trend and interannual variability of sea level near the West African coast

Arame Dièye[1,2]*, Bamol Ali Sow[1], Habib Boubacar Dieng[1], Patrick Marchesiello[2] and Luc Descroix[3]

[1]Laboratoire d'Océanographie, des Sciences de l'Environnement et du Climat (LOSEC), Université Assane Seck, Ziguinchor, Sénégal.
[2]LEGOS, University of Toulouse, IRD, CNRS, CNES, UPS, Toulouse, France.
[3]IRD UMR PALOC MNHN/IRD/Sorbonne-Université, 75231 Paris, France.

Received 21 December, 2022; Accepted 13 July, 2023

The main objectives of this study are to assess the regional distribution of sea level in terms of trend and interannual varibility and to analyze the impacts of climate variability modes such as El Niño-Southern Oscillation (ENSO) events, Tropical Atlantic Climate Modes of Variability (TACMV), North Atlantic Oscillation (NAO) on interannual variability and trend of sea level near the West Africans coasts. Indices associated with these phenomena are from the National Oceanic and Atmosphere Administration (NOAA), the Global Mean Sea Level (GMSL) time series provided by AVISO (Archiving Validation and Interpretation Satellite Oceanographic Center) and the Regional Mean Sea Level (RMSL) gridded data by CMEMS (Copernicus Marine Environment Monitoring Service). The results show that the mean regional trend of sea level is similar to the global one but the time evolution at interannual and decadal scales does not follow the pattern of global sea level. Our analysis suggests an influence of ENSO events in the Atlantic coast of West Africa. In particular, we observed negative RMSL anomalies during the two strongest El Niño events (1997-1998 and 2015) and a strong positive RMSL anomaly during the La Niña event of 2011 (the strongest over the last two decades). The analysis also reveals an influence of TACMV and NAO on the interannual sea level variability, essentially through regional Sea Surface Temperature (SST) changes. The study shows that a time series of at least 10 years is required to estimate the trend in sea level rise in West Africa. Sub-decadal trends, primarily reflect natural climate modes, rather than variations in climate change. This study also shows that the distribution of sea level rise in the West African region is heterogeneous with higher values near the coast of West Africa and near the equator.

Key words: West Africa, Sea level rising, Regional sea level variability, Climate Variability Modes, sea level interannual variability.

INTRODUCTION

Sea level rise due to anthropogenic global warming is now considered undeniable as all studies (Ablain et al., 2017; Dieng et al., 2017; Cazenave et al., 2018; Dieng et al., 2021) based on direct measurement techniques such as satellite observation and tide gauge recording reveal that the Global Mean Sea Level (GMSL) is rising. Since 1993, satellite altimetry missions have delivered accurate sea level measurements, allowing the monitoring of sea

level variations on different spatial and temporal scales (Pujol et al., 2016; Ablain et al., 2017; Legeais et al., 2018).

They estimate anaverage rate of 3.1 ± 0.3 mm/yr and an acceleration of 0.1 mm/yr² of the GMSL rise from 1993 to present (Cazenave et al., 2018). They also show a significant regional variability, with some regions experiencing greater rates (Quartly et al., 2017).

Sea level rise is a highly sensitive index of climate change (Legeais et al., 2018) because it integrates changes in several components of the climate system in response to anthropogenic forcing in addition to natural factors related to natural sources and internal climate variability (Ablain et al., 2017). The GMSL rise primarily reflects ocean warming (through thermal expansion of sea water) and land ice melting, two processes that result from anthropogenic global warming (Church et al., 2013). However, at regional scale, sea level rise is also affected by regional processes leading to large variations in temperature, currents, winds, precipitation and air pressure (Fu et al., 2019). Regional studies are therefore important to better understand the sea level variations and their relation to climate change.

West Africa, our study area, is not immune to the negative effects of sea level rise. Its impacts are increasingly noticeable and felt. Many African coastal countries are vulnerable to sea level rise, particularly where large growing cities with a high population density are situated in the coastal zone (Nicholls et al., 2008; Hinkel et al., 2012; Dada et al., 2021). Coastal risks are primarily related to hazards such as flooding and coastal erosion, associated with mean sea level rise but also with storm surges and large waves, and are particularly acute when there is significant human development along the coast (Thior et al., 2019). However, there are large gaps in the knowledge of flooding and erosion processes and on the available in-situ data in West Africa. There are only six tide gauge time series available (Dakar, Nouakchott, Palmeira, Lagos, Sonora and Takoradi) and they are difficult to use for various reasons: (1) there are gaps in the time series; (2) the gauges are not connected to a Global Positioning System (GPS) that can correct errors related to vertical movements of the earth, and (3) the measurement periods do not coincide. Therefore, satellite data are currently the only way to study the regional distribution of sea level, which are used in this paper.

Altimetry data have greatly improved near the coasts in recent years. Improvements resulted from recent altimetry missions such as Geosat follow-on (GFO), CRYOSAT-2 and HY-2A, which have been combined with older missions (Topex/Poseidon and Jason-1/2/3). In West Africa, several studies have been conducted for the validation of these coastal altimetry products (Cipollini et al., 2017; Dieng et al., 2019; Marti et al., 2021). In the present study, the CMEMS (Copernicus Marine Environment Monitoring Service) gridded data, DUACS DT version (DT2018) were used, which shows a great improvement in coastal areas compared to DT2014 (Taburet et al., 2019), thanks to the efforts of the DUACS (Data Unification and Altimeter Combination System) teams and to the recent altimetry missions mentioned above. Thus, our main objective is to take advantage of this progress to improve our understanding of sea level variations in West Africa in relation to the GMSL. The effect of climate variability modes on the interannual variability and trend estimation of sea level in the region will also be studied. First, we compared the sea level variations in West Africa with those of the GMSL in terms of interannual variability and trend. Then, we analyzed the effect of climate modes: El Niño-Southern Oscillation (ENSO), Tropical Atlantic Climate Modes of Variability (TACMV), North Atlantic Oscillation (NAO) and of the Sea Surface Temperature (SST) on interannual sea level variations in West Africa. The study identified the modes of climate variability that have the most significant impact on sea level variations over the altimeter period 1993-2019. Finally, we analyzed the spatial variability of sea level rise and the influence of interannual sea level variability on its estimation.

STUDY AREA, DATA AND METHODS

Our study area is the eastern part of the tropical Atlantic, near the West African coasts from Congo to Western Sahara (5°S - 25°N and 35°W – 20°E; Figure 1). In this study, we used several sources of data, that is, altimetric data and climate indices. For the satellite altimetry data, we used two different products available over the period 1993-2018:

(1) The GMSL (Global Mean Sea Level) time series provided by AVISO (Archiving Validation and Interpretation Satellite Oceanographic Center) is based on the combination of the reference missions (Topex/ Poseidon, Jason-1, -2 and -3) and the auxiliary missions (ERS-1,-2, Envisat and Saral/Altika) and is obtained by geographically averaging the sea level data between 66°S and 66°N.

(2) The CMEMS (Copernicus Marine Environment Monitoring Service) gridded data, version DT2018, are based on a larger set of altimetry missions by adding to the data of the reference and complementary missions mentioned above a complementary mission (Sentinel-3A) and opportunity missions (GFO, CRYOSAT-2 and HY-2A). These data are dedicated to the study of regional sea level variations and are provided daily on a 1/4° x 1/4° grid and on a latitudinal range from 82°S to 82°N. We applied monthly averaging on the data to remove residual high temporal frequencies, particularly related to ocean tide and atmospheric variability (Dieng et al., 2021). When time series are used to estimate interannual variability and trend, annual and semi-annual signals are removed

*Corresponding author. E-mail: dieyearame91@gmail.com. Tel: +221773205117.

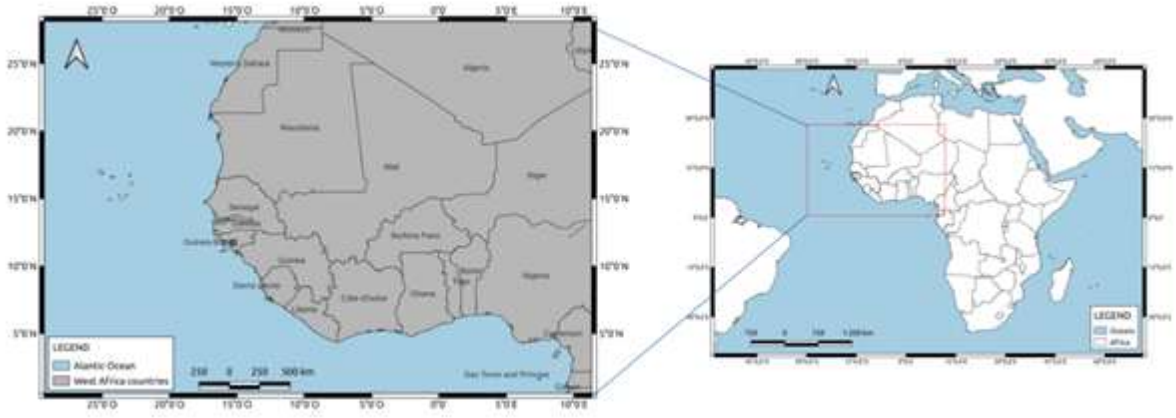

Figure 1. Map of localization of the study area.
Source: Authors

by filtering 12- and 6-month sinusoids. Regarding the modes of climate variability, we used a variety of climate indices that can have impacts on sea level variations:

(i) ENSO is a natural phenomenon that occurs in the tropical Pacific when the surface water temperature rises above 0.5 °C from normal over a period of five consecutive months due to a weakening of the trades winds that cause warm water to move east. The choice to look at the impact of ENSO on the RMSL is motivated by several studies showing a global impact on the water cycle, in particular on the interannual variability of the GMSL with strong positive anomalies during its warm phase (El Nino) and negative anomalies during its cold phase (La Nina) (Nerem et al., 2010; Llovel et al., 2010, 2011; Boening et al., 2012; Fasullo et al., 2013; Cazenave et al., 2014; Dieng et al., 2014, 2017). To characterize this phenomenon, we used 2 indices, namely the Southern Oscillation Index (SOI) and the Multivariate ENSO Index (MEI) that most characterize these events (Dieng et al., 2014). The SOI is a normalized index based on sea level pressure differences observed between Tahiti and Darwin (in Australia). The MEI is an empirical orthogonal function (EOF) time series that combines six main climate variables in the tropical Pacific: sea level pressure, zonal and meridional surface wind components, sea surface temperature, surface air temperature and total cloud fraction. The positive/negative phases of the MEI/SOI correspond to an El Niño event and negative/positive phases of the MEI/SOI correspond to La Niña.

(ii) For TACMV, we used several indices that characterize the climatic variability of the tropical Atlantic, that is, in order of importance, the Atlantic Meridian Mode (AMM), the Equatorial Atlantic (EA), the Atlantic Multidecadal Oscillation (AMO) and the Tropical Northern Atlantic (TNA). Indeed, the Eastern Tropical Atlantic, which includes our study area (West Africa), is a region of strong climatic modes of variability on interannual to decadal time scales. On the interannual scale, two modes are dominant: the Atlantic equatorial mode or Atlantic Niño and the inter-hemispherical mode or the meridian mode. The Atlantic Meridional mode is the statistically dominant mode of tropical Atlantic (Nobre and Shukla, 1996; Chang et al., 1997; Chiang and Vimont, 2004). This mode manifests itself as variations in SST in the northern and southern parts of the tropical Atlantic basin, across the Inter-tropical convergence zone (ITCZ) and it is described by the AMM index. Atlantic Niño appears every two and four years on average and presents hot and cold episodes (Atlantic Niño / Atlantic Niña), similar to that of the Pacific (El Niño - hot episode / La Niña - cold episode). However, due to the narrowness of the Atlantic basin, the oscillations are not as strong as those in the Pacific. Atlantic Niño is also characterized by a change of wind regime in the west of the basin, by a change of SST in the Gulf of Guinea and by variations of sea level slope in the equatorial band (AWO et al., 2018) and is described by the EA index. The other modes of variability in the North Atlantic basin are the North Atlantic Oscillation described by the NAO index and the Atlantic Multidecadal Oscillation described by the AMO index.

The AMM indice is calculated over the area (21°S-32°N and 74°W-15°E) by applying Maximum Covariance Analysis (MCA) to the Sea surface Temperature (SST) and the zonal and meridional components of the 10-m wind field over the time period 1950-2005, using the NCEP/NCAR Reanalysis. The EA indice is calculated over (6°N-6°S and 30°W-10°E) and produced at https://psl.noaa.gov/forecasts/sstlim/ using SST ERSST V3. The AMO indice represent the average SST anomaly over O°-80°N, calculated using the Kalplan SST V2. The TNA represents the anomaly of the mean monthly SST over the area (5.5°N - 23.5°N and 15°W-57.5°W), calculated using HadISST and NOAA OI 1x1 datasets. The NAO indice characterizes the difference of sea level pressure between the Subtropical High (Azores) and the Subtropical Low (Iceland). It is manifested by opposite profiles of temperature and precipitation anomalies and is obtained by projecting the NAO loading pattern to the daily anomaly 500 millibar height field over 0°-90°N (https://www.ncei.noaa.gov/access/monitoring/nao/). The Atlantic Multidecadal Oscillation occurs over periods of 60 to 80 years and is manifested by SST anomalies in the North Atlantic between 0°N-80°N.

The TNA, ENSO and TACMV indices are from: https://psl.noaa.gov/data/climateindices/lit/ and the NAO indice is available from the following link: https://www.cpc.ncep.noaa.gov/products/precip/Cwlink/pna/nao.shtml.

RESULTS AND DISCUSSION

The main objective of this study is to investigate the regional distribution of sea level in terms of interannual variability and trend. Thus, we identified the modes of climate variability in the Atlantic basin, but also in the Pacific (ENSO), which could have a significant impact on sea level variations and trend estimation over the altimeter

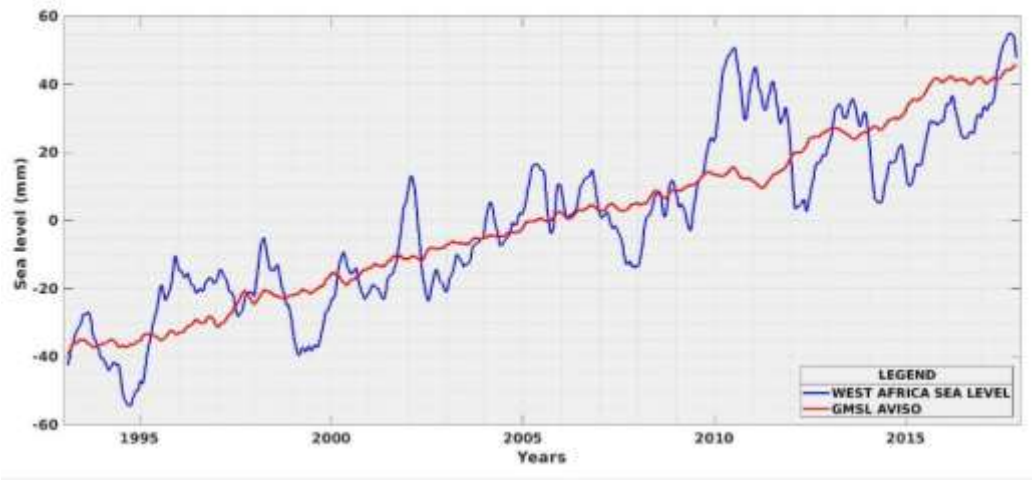

Figure 2. Regional Mean Sea Level (RMSL, in blue) from CMEMS grided data, version DT2018, and Global Mean Sea Level (GMSL) from AVISO (red). Annual and semi-annual cycles are removed and the series are smoothed over three months.
Source: Authors

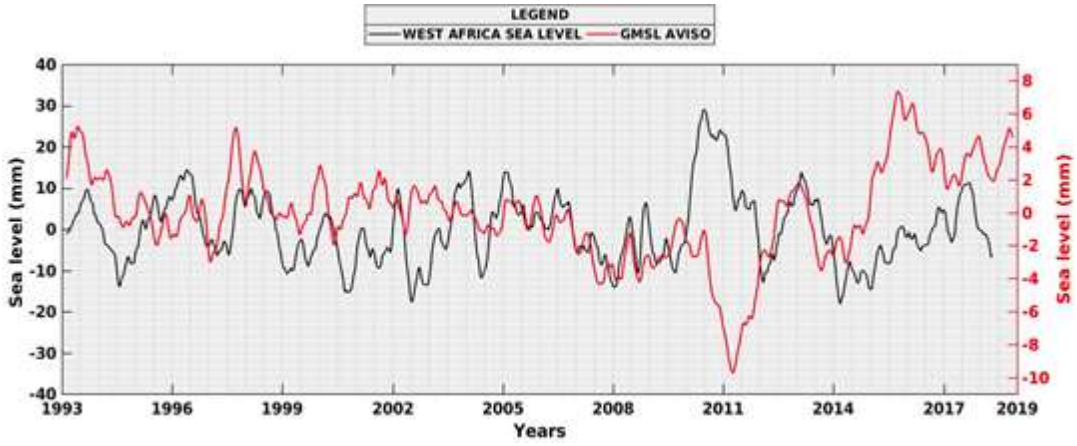

Figure 3. Interannual variations of sea level near the West African coasts and that of GMSL over the periods 1993-2018 and 1993-2019, respectively. The linear trend as well as the annual and semi-annual cycles are removed and the series are smoothed over three months. Note the different scales for the two curves.
Source: Authors

period 1993-2018.

Comparison between global and West African sea level variations

Figure 2 shows the time series of altimetry-based mean sea level variations over the period 1993-2018, at the global (GMSL) and regional (RMSL) scales. We observed a very similar trend between GMSL and RMSL, which is about 3.1 mm/year over the period 1993-2018. However, in terms of interannual variability, we noted a very large difference between GMSL and RMSL. The latter presents significant fluctuations around the trend that can reach 30 mm, that is, three times those observed on the GMSL. Interannual fluctuations are shown again in Figure 3 with linear trends removed from the time series. The differences in fluctuation can be explained by a more pronounced regional variation in the tropical Atlantic compared to the global ocean where regional variations tend to cancel out between ocean basins. We also noted that the largest interannual fluctuations are observed over the last decade compared with the earlier altimetry period. This can be related to the intensification of natural climate variability modes that has occurred for more than a decade, as suggested by Cazenave et al. (2014).

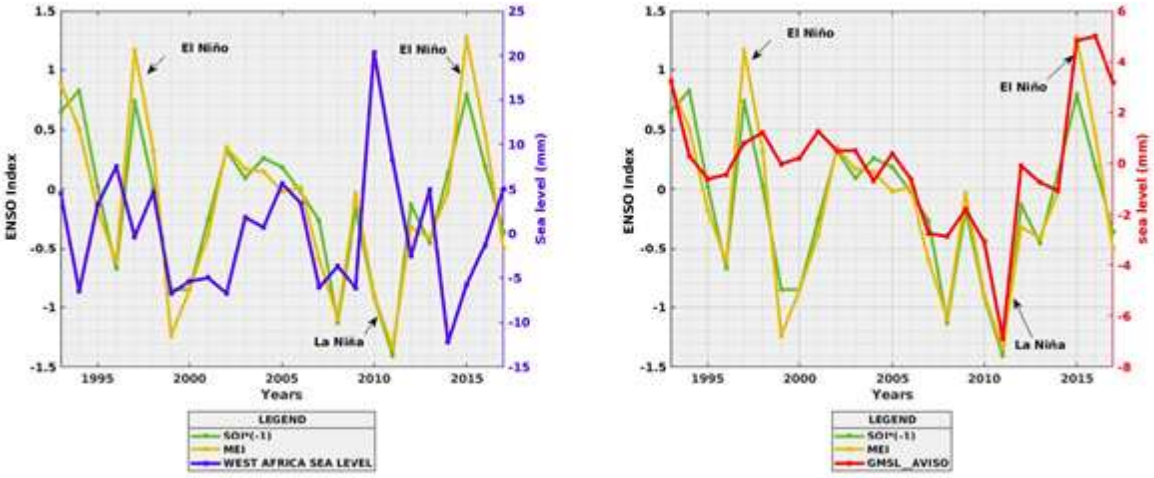

Figure 4. The ENSO indices (SOI and MEI) overlaid on the interannual variability of West Africa (to the left) mean sea level (WAMSL) and (on the right) of global mean sea level (GMSL) over the period 1993-2017.
Source: Authors

Influence of ENSO on the interannual sea level variability in West Africa

In order to analyze the influence of the ENSO phenomenon on the interannual variability of sea level in West Africa, Figure 4 presents the MEI and SOI indices (SOI is multiplied by -1 because pressure variations are inversely proportional to temperature variations). We observed negative RMSL anomalies during the two strongest El Niño events (1997-1998 and 2015) and a positive RMSL anomaly during the La Niña event of 2011 (the strongest over the last two decades). Therefore, as opposed to GMSL, RMSL has positive sea level anomalies during La Niña and negative anomalies during El Niño. However, RMSL only responds to strong ENSO events that have global impacts. This result suggests an influence of strong ENSO events beyond the Pacific basin to the Atlantic coast of West Africa. This is in agreement with previous studies (Nerem et al., 2010; Llovel et al., 2011; Boening et al., 2012; Fasullo et al., 2013; Cazenave et al., 2014; Dieng et al., 2017) showing a modification of the global water cycle with an excess of water over the ocean and a deficit over the continents (for example, in the Amazon basin) during El Niño and the opposite during La Niña. However, we are unable to explain by what mechanism strong El Niño/La Niña events can lead to negative/positive anomalies of RMSL, in opposition to GMSL.

Influence of TACMV and NAO on the interannual sea level variability in West Africa

In order to analyze the effect of the TACMV and of the NAO on the interannual sea level variability in West Africa, their associated indices (AMM, EA, NAO*(-1) and AMO) were used. Figures 5 and 6 show that the sea level peak observed in 2011 coincides with a positive phase of the AMM, EA, NAO and AMO. This particular year coincides with very high SST anomalies in the Atlantic basin (at the same time in the North Atlantic, North tropical Atlantic and in the Gulf of Guinea). Also, the correlations obtained between the interannual sea level variability in West Africa and the two main dominant climatic modes in the Atlantic (AMM and NAO indices) are quite high (correlation (NAO) = 0.51; correlation (AMM) = 0.65) and significant (P-value (NAO) = 0.0086; P-value (AMM) = $4.985\ 10^{-4}$). This suggests that the TACMV and NAO have a major influence on the interannual sea level variability in West Africa, in addition to ENSO, which shows an impact during strong events.

Influence of SST Variability on the interannual sea level variability in West Africa

In order to analyze the impact of SST variations, we compared the Tropical North Atlantic (TNA) SST anomaly index (calculated with SST in the box 55°W to 15°W and 5°N to 25°N) with the sea level interannual variability in West Africa (Figure 7).

We observed a strong correlation (correlation=0.68) that is very significant (P-value (TNA) $=1.797e^{-04}$) between these two variables. This may suggest that SST interannual variations control a large part of the interannual sea level variability through regional thermal expansion. This would thus be the main process through which the natural modes of climate variability affect the region.

Spatial variability of sea level rise in West Africa

Figure 8a illustrates regional variations in sea level trend

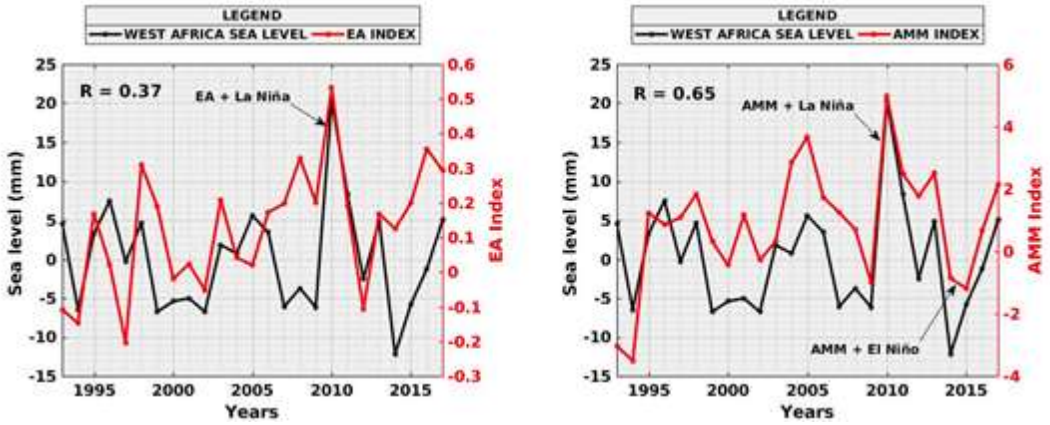

Figure 5. Interannual variability of sea level in West Africa over the period 1993-2017 and the TACMV indices (AMM and EA).
Source: Authors

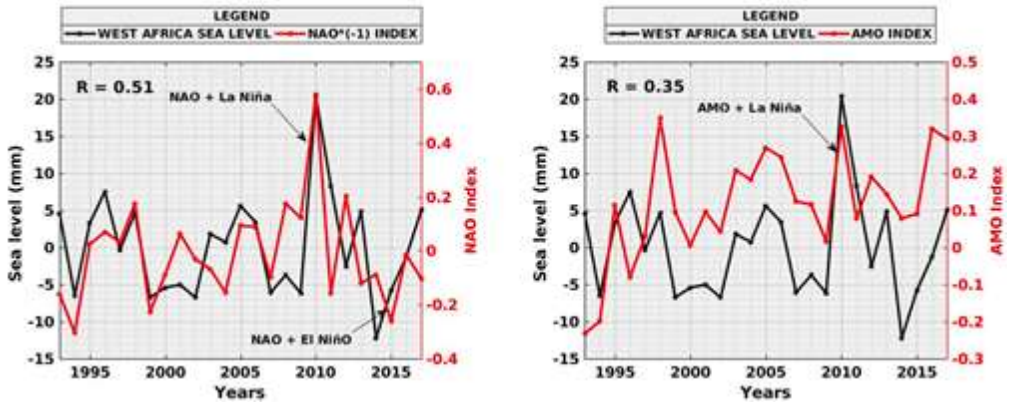

Figure 6. Interannual variability of sea level in West Africa over the period 1993-2017 and the North Atlantic modes of variability indices (NAO and AMO index).
Source: Authors

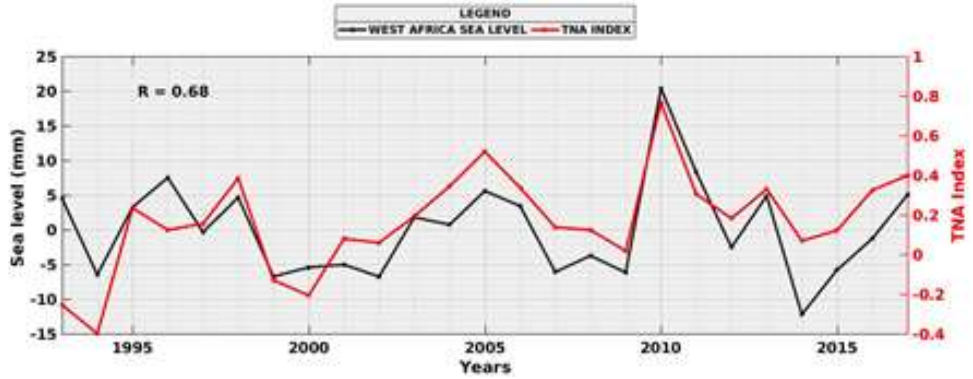

Figure 7. Interannual sea level variability in West Africa over the period 1993-2017 and the TNA index (SST index).
Source: Authors

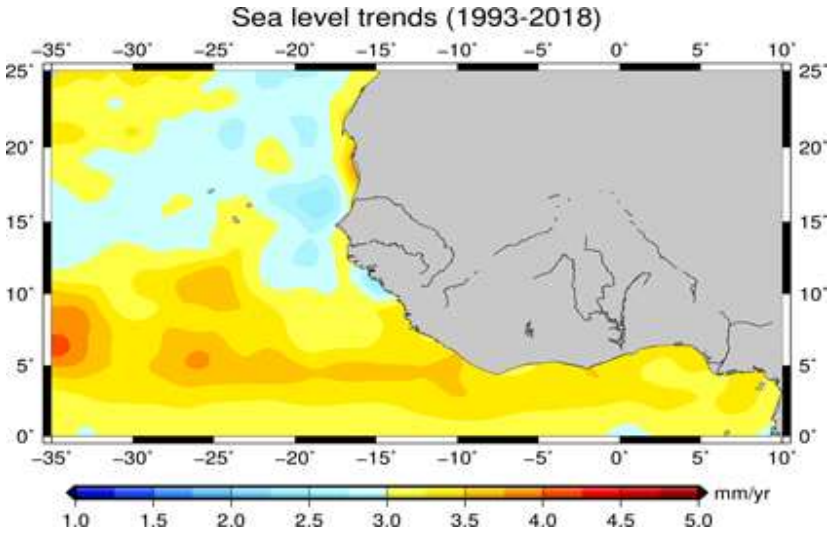

Figure 8a. Map of West African sea level rise in mm/year from the CMEMS (Copernicus Marine Environment Monitoring Service) gridded data, version DT2018, over the period 1993-2018.
Source: Authors

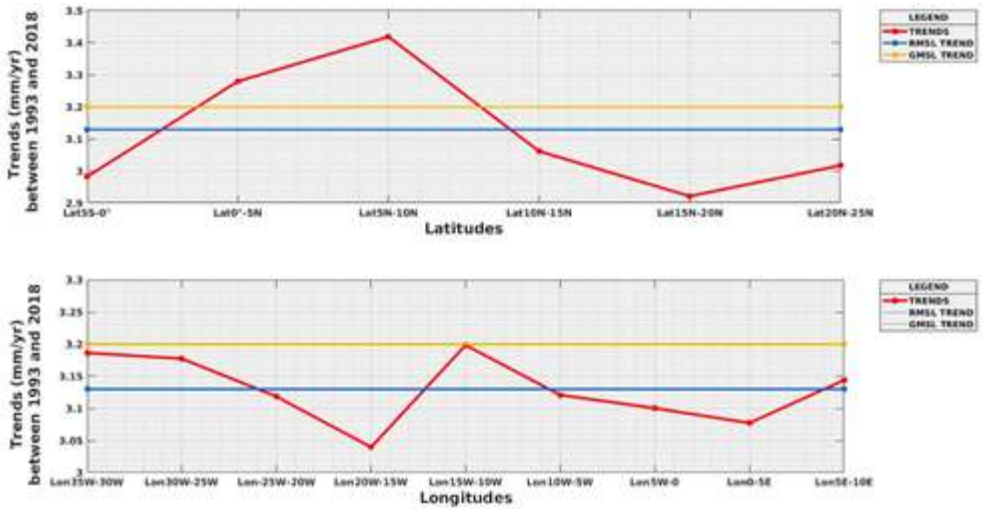

Figure 8b. (Red curves) Latitudinal (top) and longitudinal (bottom) variability of sea level rise near the West African coasts between 1993 and 2018. The mean GMSL and RMSL trends are shown for comparison.
Source: Authors

over the period 1993-2018 near the West African coast. It shows a non-uniform distribution of the regional sea level rise near the West African coast. To go further, we analyzed the spatial variability of sea level rise by bands (that is latitudinal and longitudinal variability). Figure 8b presents an SLR (Sea Level Rise) analysis on 5° latitude and 5° longitude bands, showing a strong spatial variability. Low latitudinal bands (0°N-5°N) and (5°N-10°N) are marked by a high rate, greater than that of RMSL (3.13 mm/yr) or GMSL (3.1 mm/yr). On the contrary, at higher latitude, the rate is lower than the regional and global means. Longitudinal variability in SLR increases from the coastal to the offshore zone. This is consistent with Marti et al. (2021) who show that SLR near the West African coast is significantly different from that offshore. In our data, the rate is weaker in the band

Table 1. Errors on the regional trend at different periods.

Periods	Trends (mm/year)	Errors	Errors (%)
5 years			
1993-1997	7.1571	0.2469	24
1998-2002	3.0124	0.2402	24
2003-2007	6.7458	0.1387	13
2008-2012	13.0690	0.2347	23
2013-2018	4.2029	0.1705	17
6 years			
1993-1998	5.6990	0.1634	16
1999-2004	5.5926	0.1554	15
2005-2010	-0.0944	0.1433	14
2011-2016	-2.3257	0.1696	16
2013-2018	4.2029	0.1705	17
7 years			
1993-1999	5.2441	0.1157	11
2003-2009	1.7458	0.1080	10
2012-2018	4.9518	0.1207	12
8 years			
1993-2000	2.4602	0.1142	11
2002-2009	2.1982	0.0919	9
2011-2018	1.9761	0.1146	11
9 years			
1993-2001	2.5953	0.0876	8
2010-2018	0.22	0.1057	10
10 years			
1993-2002	2.7305	0.0703	7
2009-2018	1.4225	0.0906	9
11 years			
1993-2003	2.8061	0.0627	6
2008-2018	2.2860	0.077	7
12 years			
1993-2004	2.6847	0.0522	5
2007-2018	3.0626	0.0695	6
13 years			
1993-2005	2.8995	0.0442	4
2006-2018	2.9119	0.0585	5

Source: Authors

(15°W-20°W) near the coasts of the Sahel and Sub-Saharan Africa areas. In the Gulf of Guinea, the rate is high in both the eastern zone (10E-5E, near the coasts of Cameroun and Equatorial Guinea) and western zone (15W-10W, near the coasts of Liberia). They are even higher than the regional rate while in the middle of the Gulf (10W to 5E, near the coast of Côte d'Ivoire, Ghana, Togo, Benin and Nigeria) the rate is lower.

Influence of interannual sea level variability on SLR estimation near the coast of Africa

Given the importance of interannual sea level variability near the West African coast, it is important to estimate its impact on the calculation of the RMSL trend, in order to determine the minimum period to be used for a significant estimation in our study area. To do this, we recalculated the RMSL trend over periods of 5 to 13 years. For example, the 5-year periods correspond to 1993-1997, 1998-2002, 2003-2007, 2008-2012 and 2013-2018. The trends with associated statistical errors are shown in Table 1. As expected, the error is smaller when the length of the time series increases. If we assumed an acceptable statistical error to be less than 0.1 mm/yr (or 10% of SLR), a reliable estimation of SLR in West Africa requires at least a time series of ten years. For smaller series, year to year anomalies can strongly impact the estimation. For example, the high rate obtained over the period 2008-2012 (13.07 mm/yr) can be explained by the large positive sea level anomaly (> 30 mm) of 2010-2011. Similarly, the negative trends for 2005-2010 (-0.09 mm/yr) and 2011-2016 (-2.33 mm/yr) can be explained by the negative sea level anomalies of 2008 and 2012-2015 respectively (Figure 3 and Table 1). Based on the previous error analysis, we now look at the SLR trend changes in West Africa using 10 years' time periods and comparing them to that of GMSL. We considered two cases: (1) successive trends, described by the first, second and last decades of the altimetric measurements (that is, 1993-2002, 2001-2010 and 2009-2018); (2) running trend, described by decades starting at three-year intervals (that is, 1993-2002, 1995-2004, 1997-2006, 1999-2008). Figure 9 shows that the trends are not constant or linear in time and the West African evolution do not correlate with that of GMSL. For example, the running trend shows an acceleration of RMSL in 1995-2004, 1997-2006 and 1999-2008 as opposed to GMSL (the rates in West Africa are: 1.73 mm/yr, 3.70 mm/yr and 4.09 mm/yr; and for GMSL: 3.42 mm/yr, 3.22 mm/yr and 3.04 mm/yr). We also had periods when RMSL is slowing down in West Africa (2003-2012, 2005-2014, 2007-2016 and 2009-2018) and speeding up in GMSL (the rates in West Africa are: 5.18 mm/yr, 3.70 mm/yr 2.62 mm/yr and 1.42 mm/yr; for GMSL: 2.59 mm/yr, 3.12 mm/yr 4.00 mm/yr and 4.49 mm/yr). With respect to changes in the successive decades (Figure 9, right panel), it also appears that regional and global trend changes are

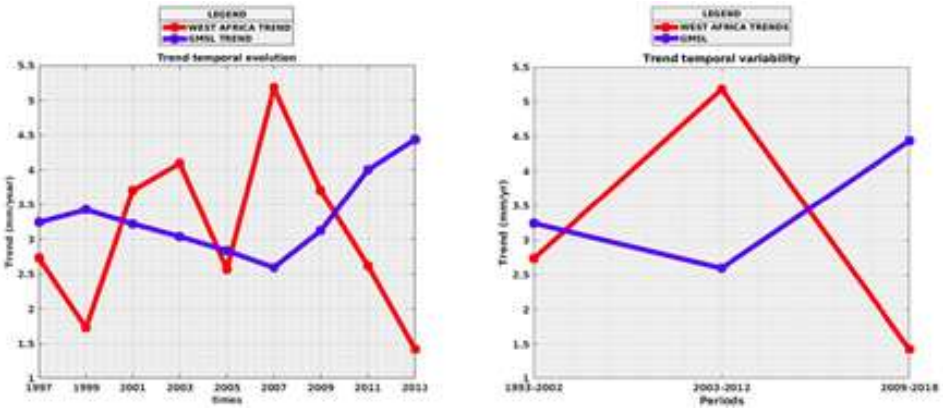

Figure 9. SLR running trend (left) and successive trend (right) over decades in West Africa (red) and GMSL (blue).
Source: Authors

anticorrelated, although the small number of decades available does not permit statistical significance. In the first decade of altimetric measurement, the RMSL in West Africa is lower than that of GMSL (+2.73 mm/yr versus +3.24 mm/yr). Then, during the second decade, it is twice larger (+5.18 mm/yr versus +3.59 mm/yr). Finally, over the last decade (2009-2018), there has been a considerable slowdown in RMSL in West Africa while there has been a global acceleration (+1.4 mm/yr versus +4.4 mm/yr). This apparent anticorrelation is reminiscent of that observed in the interannual variability (Figure 3) and shows the impact of this variability on the estimation of RMSL. This result is in agreement with Cazenave et al. (2014) who suggested removing the variability associated with natural climate modes for a better estimation of the sea level trend due to climate change.

Conclusions

This study aimed to improve the understanding of the current variations of sea level near the West African coasts. To that end, the study re-examined the spatial variability of the regional sea level trend and described its evolution over time using GMSL time series provided by AVISO and CMEMS gridded data, version DT2018 (specifically dedicated to regional sea level studies). The study shows that the distribution of sea level trend is not uniform in the region of West Africa and its evolution is not linear over time. In addition, if the mean tendency is similar in regional and global sea level, the time evolution of RMSL at interannual and decadal scales does not follow that of GMSL. This paper identified some factors related to global and regional internal (natural) climate variability that may have an influence on sea level interannual variability and trend in West Africa. The analysis is based on comparison of RMSL and GMSL with several indices associated with these climate modes. The study shows that regional climate variability, particularly that affecting regional temperature, has a strong influence on the trend and interannual variability of sea level in West Africa. Strong ENSO events are particularly efficient contributors. However, in the future it would be interesting to also analyze the influence of other environmental factors such as wind, precipitation and atmospheric pressure. The West African sea level budget could also be improved by identifying the main climatic factors contributing to regional sea level rise, which would address the lack of in situ data in the region.

CONFLICT OF INTERESTS

The authors have not declared any conflict of interests.

ACKNOWLEDGEMENT

The authors are grateful for the financial assistance given by the European Union, DeSIRA project ‘Mangroves, mangrove rice and mangrove people: sustainably improving rice production, ecosystems and livelihoods’ (Grant Contract FOOD/2019/412-700).

REFERENCES

Ablain M, Legeais JF, Prandi P, Fenoglio-Marc L, Marcos M, Benveniste J, Cazenave A (2017). Satellite altimetry based sea level at global and regional scales. Surveys in Geophysics 38:9-33.

Awo FM, Alory G, Da-Allada CY, Delcroix T, Jouanno J, Kestenare E, Baloïtcha E (2018). Sea surface salinity signature of the tropical Atlantic interannual climatic modes. Journal of Geophysical Research: Oceans 123:7420-7437.

Boening C, Willis JK, Landerer FW, Nerem RS (2012). The 2011 La Niña: so strong, the oceans fell. Geophysical Research Letters 39:L19602. DOI: 10.1029/ 2012GL053055.
Cazenave A, Dieng HB, Meyssignac B, Schuckmann KV, Decharme B, Berthier E (2014). The Rate of Sea-Level Rise. Nature. Climate Change 4(5):358-361.
Cazenave A, Palanisamy H, Ablain M (2018). Contemporary Sea level changes from satellite altimetry; what have we learned? What are the new challenges? Advances in Space Research 62(7):1639-1653.
Chang P, Ji L, Li H (1997). A decadal climate variation in the tropical Atlantic Ocean from thermodynamic air-sea interactions. Nature 385(6616):516-518.
Chiang JCH, Vimont DJ (2004). Analogous Pacific and Atlantic Meridional Modes of Tropical Atmosphere-Ocean Variability. Journal of Climate 17(21):4143-4158.
Church JA, Clark PU, Cazenave A, Gregory JM, Jevrejeva S, Levermann A, Merrifield MA, Milne GA, Nerem RS, Nunn PD, Payne AJ, Pfeffer WT, Stammer D, Unnikrishnan AS (2013). Sea level change: Climate Change 2013: The Physical Science Basis, edited by: Stocker, T. F., Qin, D., Plattner, G.-K., Tignor, M., Allen, S. K., Boschung, J., Nauels, A., Xia, Y., Bex, V., and Midgley, P. M., 2013. Contribution of Working Group I to the Fifth Assessment Report of the Intergovernmental Panel on Climate Change. Cambridge University Press, Cambridge, United Kingdom and New York, NY, USA.
Cipollini P, Francisco M, Svetlana C, Melet JA, Prandi P (2017). Monitoring Sea Level in the Coastal Zone with Satellite Altimetry and Tide Gauges. Surveys in Geophysics 38(1):33-57.
Dada O, Almar R, Morand P, Menard F (2021). Towards West African coastal social-ecosystems sustainability: Interdisciplinary approaches. Ocean and Coastal Management 211:105746.
Dieng HB, Cazenave A, Gouzenes Y, Sow BA (2021). Trends and inter-annual variability of altimetry-based coastal sea level in the Mediterranean Sea: Comparison with tide gauges and models. Advances in Space Research 68:3279-3290.
Dieng HB, Cazenave A, Meyssignac B, Ablain M (2017). New estimate of the current rate of sea level rise from a sea level budget approach. Geophysical Research Letters 44:3744-3751.
Dieng HB, Cazenave A, Meyssignac B, Henry O, Schuckmann KV, Palanisamy H, Lemoine JM (2014). Effect of La Niña on the global mean sea level and North Pacific Ocean mass over 2005-2011. Journal of Geodetic Science 4:19-27.
Dieng HB, Dadou I, Léger F, Morel Y, Jouanno J, Lyard F, Allain D (2019). Sea level anomalies using altimetry, model and tide gauges along the African coasts in the Eastern Tropical Atlantic Ocean: Inter-comparison and temporal variability. Advances in Space Research 68(2):534-552.
Fasullo JT, Boening C, Landerer FW, Nerem RS (2013). Australia's unique influence on global sea level in 2010–2011. Geophysical Research Letters 40(60):4368-4373.
Fu Y, Zhou X, Zhou D, Sun W, Jiang C (2019). Sea level trend and variability in the south china Sea. ISPRS Annals of the Photogrammetry, Remote Sensing and Spatial Information Sciences, IV-2/W5 pp. 589-593.
Hinkel J, Brown S, Exner L, Nicholls RJ, Vafeidis AT, Kebede AS (2012). Sea-level rise impacts on Africa and the effects of mitigation and adaptation: an application of DIVA. Regional Environmental Change 12:207-224.
Legeais JF, Ablain M, Zawadzki L (2018). An improved and homogeneous altimeter sea level record from the ESA Climate Change Initiative. Earth System Science Data 10(1):281-301.
Llovel W, Becker M, Cazenave A, Crétaux JF, Ramillien G (2010). Global land water storage change from GRACE over 2002–2009; Inference on sea level. C. R. Geoscience 342(3):179-188.
Llovel W, Becker M, Cazenave A, Jevrejeva S, Alkama R, Decharme B, Douville H, Ablain M, Beckley B (2011). Terrestrial waters and sea level variations on interannual time scale. Global Planet Change 75(1-2):76-82.
Marti F, Cazenave A, Birol F, Passaro M, Léger F, Niño F, Almar R, Benveniste J, Legeais JF (2021). Altimetry-based sea level trends along the coasts of Western Africa. Advances in Space Research 68(2):504-522.
Nerem RS, Chambers DP, Choe C, Mitchum GT (2010). Estimating Mean Sea Level Change from the TOPEX and Jason Altimeter Missions. Marine Geodesy 33(S1):435-446.
Nicholls RJ, Hanson S, Herweijer C, Patmore N, Hallegatte S, Corfee-Morlot J, Chateau J, Muir-Wood R (2008). Ranking port cities with high exposure and vulnerability to climate extremes: exposure estimates. OECD Environment Working Papers, No. 1, OECD publishing, 3-62, DOI: 10.1787/011766488208
Nobre P, Shukla J (1996). Variations of sea surface temperature, wind stress, and rainfall over the tropical Atlantic and South America. Journal of Climate 9:2464-2479.
Pujol MI, Faugère Y, Taburet G, Dupuy S, Pelloquin C, Ablain M, Picot N (2016). DUACS DT2014: the new multi-mission altimeter data set reprocessed over 20 years. Ocean Science 12:1067-1090.
Quartly GD, Legeais JF, Ablain M, Zawadzki L, Fernandes MJ, Rudenko S, Carrère L, García PN, Cipollini P, Andersen OB, Poisson JC, Mbajon Njiche S, Cazenave A, Benveniste J (2017). A new phase in the production of quality-controlled sea level data. Earth System Science Data 9:557-572.
Taburet G, Sanchez-Roman A, Ballarotta M, Pujol MI, Legeais JF, Fournier F, Faugere Y, Dibarboure G (2019). DUACS DT2018: 25 years of reprocessed sea level altimetry products. Ocean Science 15(15):1207-1224.
Thior M, Dièye T, Sané T, Dièye El H. B, Sy O (2019). Coastline dynamics of the northern Lower Casamance (Senegal) and southern Gambia littoral from 1968 to 2017. Journal of African Earth Sciences 160:103611.

Related Journals: